Priddis low-frequency seismometer test, part 2

Kevin W. Hall (kwhall@ucalgary.ca), Malcolm B. Bertram, Gary F. Margrave and David W. Eaton

SUMMARY

CREWES acquired a low-frequency sensor comparison test dataset in 2009. The dataset was acquired using a weight drop trailer and an IVI Minivibe (2-10 Hz and 2-100 Hz linear sweeps with different sweep lengths and peak force levels) at two source points, offset by 50 meters from the ends of the north-south receiver lines. Sensors on the ground included accelerometers (DSU3 and VectorSeis), geophones (SM-24) and broadband seismometers (Trillium 240). Near-offset (50 m) traces for a single 2-100 Hz linear sweep are visually compared as 1) uncorrected, uncorrelated data, 2) converted to common units and corrected for geophone and seismometer instrument response in the velocity and acceleration of ground motion domains (as opposed to velocity and acceleration of proof mass domains). Least-squares-subtraction-scalar results are also presented. System electrical noise appears to dominate signal below about 7 Hz for all systems, likely due to the long taper used for the low frequencies (< 10 Hz) and the low power used for the sweep in order to not damage the Minivibe. We appear to have a close match (other than a multiplicative constant) down to at least 5 Hz for all recording systems and sensors.

Table 1. Known parameters for the recording systems.

System	Data Units	Sensitivity		Source
Trillium	μV	1168.2	V/m/s	Nanometrics (2008)
Aries	V	20.5	V/m/s at 0.7 damping	Hons (2008)
Scorpion	g			Vince Rodych (pers. comm.)
Sercel	mV	408	$mV/m/s^2$	Jim Roy (pers. comm.)

The transfer functions used to correct for geophone and seismometer instrument response with velocity output are given by Equations 1 (geophone) and 2 (seismometer), where H is the frequency domain representation of the transfer function, S is the sensitivity (Table 1), ω is frequency, j is the square root of negative one, λ is the damping ratio of the geophone and ω_0 is the natural frequency (Hons, 2008), z_a and p_b are the nominal complex zeros and poles of the transfer function listed in the seismometer user manual (Nanometrics, 2008). Multiply by $j\omega$ for displacement and divide by $j\omega$ for acceleration

$$H = -S\frac{\omega^2}{-\omega^2 + 2j\lambda\omega\omega_0 + \omega_0^2} \quad (1)$$

$$H = S\frac{\sum_{a=1}^{N}\omega - z_a}{\sum_{b=1}^{M}\omega - p_b} \quad (2)$$

ACKNOWLEDGEMENTS

The authors would like to thank the field crew, from all companies and institutions involved. Information about the Scorpion and Sercel systems provided by Vince Rodych and Jim Roy were very helpful. Continuing support of the CREWES sponsors is also gratefully acknowledged.

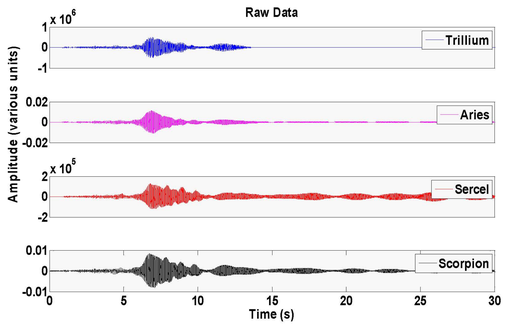

FIG. 1a. Visual comparison of vertical component, uncorrected uncorrelated data for a 30 s 2-100 Hz linear sweep with a 50 m source-receiver offset (north VP).

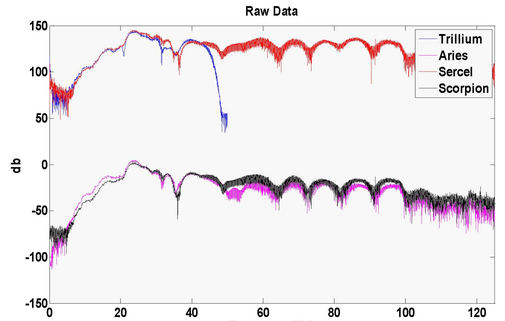

FIG. 1b. Visual comparison of vertical component, uncorrected uncorrelated data for a 30 s 2-100 Hz linear sweep with a 50 m source-receiver offset (north VP).

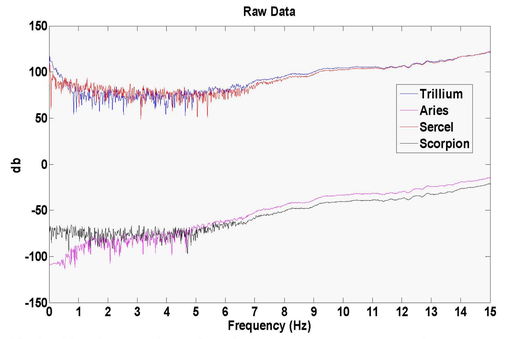

FIG. 1c. Visual comparison of vertical component, uncorrected uncorrelated data for a 30 s 2-100 Hz linear sweep with a 50 m source-receiver offset (magnified portion of Figure 1b).

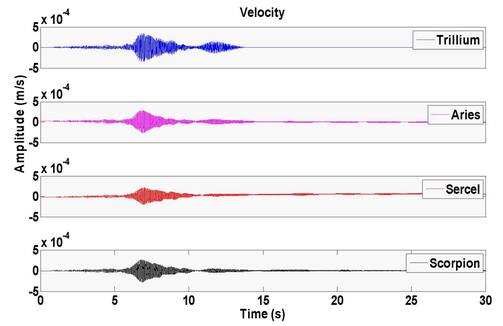

FIG. 2a. Visual comparison after converting raw data to velocity; Data corrected for geophone and seismometer instrument response.

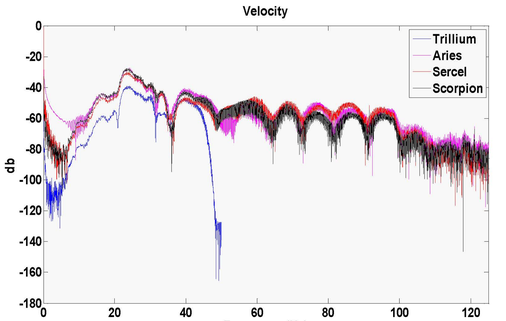

FIG. 2b. Visual comparison after converting raw data to velocity; Data corrected for geophone and seismometer instrument response.

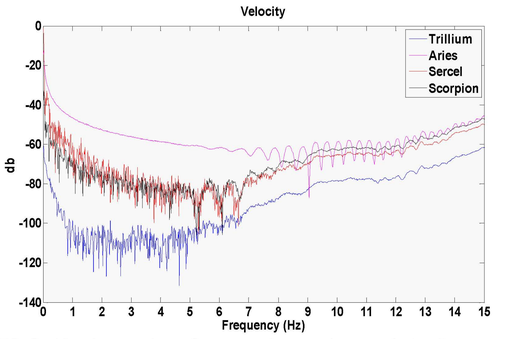

FIG. 2c. Visual comparison after converting raw data to velocity; Data corrected for geophone and seismometer instrument response. (magnified portion of Figure 2b).

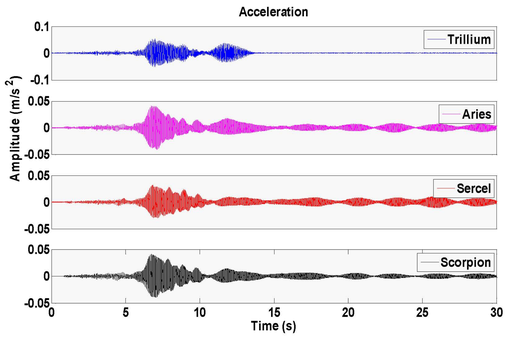

FIG. 3a. Visual comparison after converting raw data to acceleration; Data corrected for geophone and seismometer instrument response.

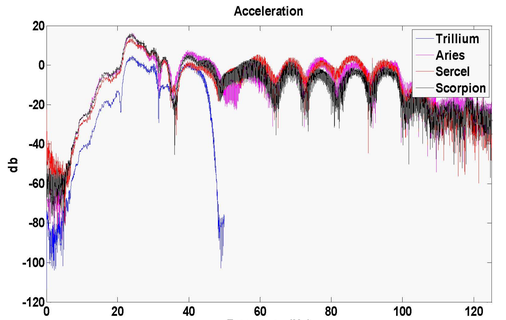

FIG. 3b. Visual comparison after converting raw data to acceleration; Data corrected for geophone and seismometer instrument response.

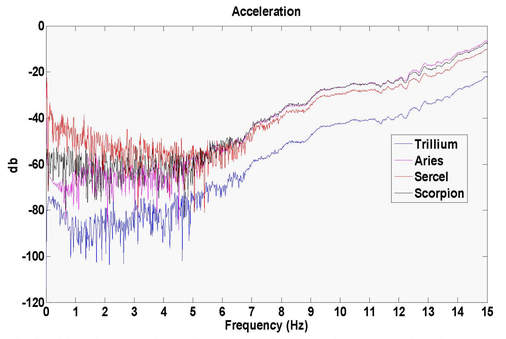

FIG. 3c. Visual comparison after converting raw data to acceleration; Data corrected for geophone and seismometer instrument response. (magnified portion of Figure 3b).

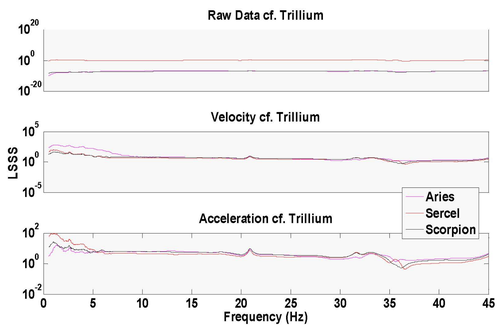

FIG. 4a. Frequency dependent Least-squares-subtraction-scalar curves for Figures 1b-3b; Data compared to Trillium.

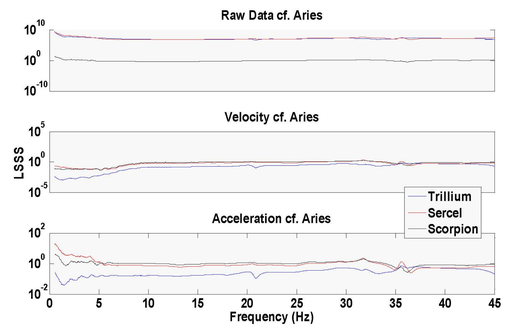

FIG. 4b. Frequency dependent Least-squares-subtraction-scalar curves for Figures 1b-3b; Data compared to Aries.

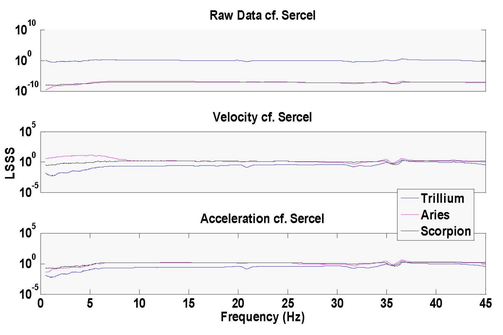

FIG. 4c. Frequency dependent Least-squares-subtraction-scalar curves for Figures 1b-3b; Data compared to Sercel.

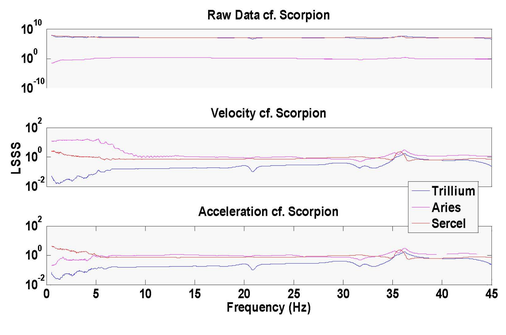

FIG. 4d. Frequency dependent Least-squares-subtraction-scalar curves for Figures 1b-3b; Data compared to Scorpion